

Synthesis of super-heavy elements in the outer crust of a magnetar

D. Basilico,¹ G. Colò,^{2,1} and Xavier Roca-Maza^{1,2,3,4}

¹*INFN, Sezione di Milano, 20133 Milano, Italy*

²*Dipartimento di Fisica “Aldo Pontremoli”, Università degli Studi di Milano, 20133 Milano, Italy*

³*Departament de Física Quàntica i Astrofísica, Martí i Franqués, 1, 08028 Barcelona, Spain*

⁴*Institut de Ciències del Cosmos, Universitat de Barcelona, Martí i Franqués, 1, 08028 Barcelona, Spain*

(Dated: March 27, 2024)

A theoretical understanding of a possible mechanism for synthesizing super-heavy elements in the outer crust of magnetars is presented. We demonstrate that such a mechanism can be present whenever the baryon density in the outer crust of a neutron star reaches values around 10^{-2} fm^{-3} . This scenario could be realized in magnetars with hypothetical large magnetic fields, $B \gtrsim 10^{18} \text{ G}$. Under such conditions, the Coulomb lattice, formed by ionized nuclei, enables a mechanism that synthesizes super-heavy elements.

I. Introduction

Neutron stars are one of the most fascinating objects in the Universe [1]. Among their many unique features, they host extremely strong magnetic fields that can be in the range of $\approx 10^{11} - 10^{14} \text{ G}$. There is no understanding of either the origin or the structure of these fields, although the simple argument of the magnetic flux conservation during the collapse of a progenitor main sequence star can lead to values of the order of $\approx 10^{12} \text{ G}$. From observations of the last decade, values up to $2.4 \times 10^{15} \text{ G}$ have been deduced [2–6]. However, even stronger values cannot be ruled out, and possible magnetic fields B up to $\approx 10^{18} \text{ G}$ have been suggested, e.g., in Refs. [7–9]. The physics of stars characterised by a strong magnetic field like the magnetars, which are a subset of neutron stars, is an active field of research, and understanding the nature and implications of this huge magnetization is a challenge for astronomy and astrophysics [10].

The outer crust of a neutron star is composed of nuclei arranged in a Coulomb lattice surrounded by ionized electrons [1, 11]. While the lattice is unaltered by the presence of magnetic fields [12], the electron energy levels are quantized according to the famous Landau-Rabi levels [13, 14]. This crucially affects the electronic contribution to the density and pressure in the outer crust if extremely large magnetic fields are present. In such conditions, the nuclear structure may be also affected. Indeed, external magnetic fields stabilize nuclei, producing an extra binding that does not increase by more than 10%–15% when the more extreme magnetic fields, $B \approx 10^{18} \text{ G}$, are taken into account [15–17].

Which nuclei can be precisely synthesized, how does the magnetic field affect this kind of “nucleosynthesis”, and what can be learnt therefrom? These are the key questions that have already been the subject of a few investigations. In particular, the works that have been published since the last decade and devoted to the effect of the magnetic field on the composition of the outer crust include Refs. [15–21]. Recently, in the work of Ref. [22], the authors have explored extremely large magnetic fields $B \gtrsim 10^{18} \text{ G}$ and suggested that, in the innermost layers

of the outer crust, with average baryon densities of about 10^{-2} fm^{-3} (cf. Fig. 3 of Ref. [22]), super-heavy elements (SHE) show up. The densities present in the outer crust are known to depend on the magnetic field. Indeed, in Ref. [18], it is shown that both the surface density as well as the neutron drip density –defining the separation with the inner crust– could experience large changes with the presence of extreme magnetic fields. As an example, for $B = 0$, the density range spans seven orders of magnitude: from $\approx 10^{-11} \text{ fm}^{-3}$, i.e. the electronic complete ionization threshold, to $\approx 10^{-4} \text{ fm}^{-3}$ i.e. the neutron drip [1, 11]. For the case of extremely large magnetic fields such as $B \sim 10^{18} \text{ G}$, such range is shrunk and shifted to larger densities (cf. Eqs. (27) and (51) as well as Fig. 2 in Ref. [18], Fig. 6 in Ref. [16], Fig. 5 and Fig. 6 in Sec. III) reaching neutron drip densities of about 10^{-2} fm^{-3} . Consequently, we can say that the presence of densities that may trigger the appearance of SHE is intimately related to the existence of a strong magnetic field.

The findings of Ref. [22], although very interesting, are not explained in simple terms. Our motivation in the present work is twofold. Not only do we want to assess if the results of [22] are confirmed if one uses different state-of-the-art nuclear mass models, but we also aim to understand the reason for the synthesis of SHE in simple and yet robust terms, in a qualitative and model-independent manner.

With that in mind, in Sec. II, we will briefly remind the theoretical general framework, but we shall also present a model for the qualitative understanding of the properties of the outer crust, valid for average baryon densities $n \sim 10^{-2} \text{ fm}^{-3}$ and extremely large magnetic fields $B \gtrsim 10^{18} \text{ G}$. This will allow us to understand the underlying physical mechanism that may produce super-heavy elements in simple yet reliable terms. In Sec. III, we will confirm our understanding by discussing numerical results obtained with a two state-of-the-art nuclear models. Our conclusions will be laid in Sec. IV.

II. Theoretical model

The outer crust is assumed to be composed of nuclei in their ground state at zero temperature, arranged in a Coulomb lattice, and of ionized electrons [1, 11, 15–21]. We consider this system to be embedded in a uniform magnetic field that extends throughout the outer crust. The equilibrium in the outer crust is established by demanding that the temperature (T), pressure (P), and chemical potential (μ), but not necessarily the average baryon density ($n \equiv A/V$ where V is the unit cell volume of the Coulomb lattice and A the mass number of the nucleus that is contained therein), are continuous functions. At $T = 0$, the Gibbs free energy per baryon (μ) and the energy of the system per baryon (ε) are related to the pressure and average baryon density as follows,

$$\mu(A, Z; P, B) = \varepsilon(A, Z; P, B) + \frac{P}{n}. \quad (1)$$

The composition (A, Z) of the outer crust for a fixed value of pressure and magnetic field (B) is determined by minimizing the Gibbs free energy per baryon $\mu(A, Z; P, B)$. Note that pressure, energy and density are related via $P = n^2 \frac{\partial \varepsilon}{\partial n}$ for a fixed number of baryons. Hence, the only unknown in the above equation is $\varepsilon(A, Z; P, B)$. The energy per baryon of the system, $\varepsilon(A, Z; P, B)$, is the sum of three independent contributions:

$$\varepsilon(A, Z; P, B) = \varepsilon_n(A, Z) + \varepsilon_e(A, Z; P, B) + \varepsilon_l(A, Z; P, B), \quad (2)$$

namely the *nuclear*, *electronic* and *lattice* energy terms, respectively. In what follows, we will use natural units with $\hbar = c = 1$, as is customary in the references that we have quoted.

The electronic contribution $\varepsilon_e(A, Z; P, B)$ would be that of a degenerate Fermi gas of relativistic electrons in the absence of a magnetic field: as is well known, the Coulomb interaction among electrons becomes negligible at the densities we are considering. However, when a uniform magnetic field B is present – directed along the z -axis in our case –, while the energy keeps a continuous dependence on the component p_z or the electron momenta, the energy levels are quantized and have energy [13, 14]

$$E^2(\nu, p_z) = p_z^2 + m_e^2 (1 + 2\nu B_\star). \quad (3)$$

Here, m_e is the electron rest mass, ν is a non-negative quantum number and $B_\star \equiv B/B_c$, with $B_c \equiv \frac{m_e^2 c^4}{e\hbar c} \approx 4.4 \times 10^{13}$ G being the magnetic field at which the electron cyclotron energy becomes equal to the electron rest mass. The highest electron momentum allowed, that is the electron Fermi momentum p_{Fe} , can be computed by setting $E(\nu, p_{\text{Fe}}) = \mu_e$ in Eq. (3):

$$\mu_e^2 = p_{\text{Fe}}^2 + m_e^2 (1 + 2\nu_{\text{max}} B_\star). \quad (4)$$

The maximum value of ν allowed, named ν_{max} , is evaluated by setting $E(\nu_{\text{max}}, 0) = \mu_e$ in Eq. (3). In other

words, the energy due to the electron coupling with the magnetic field cannot exceed the electron chemical potential μ_e . The electron density is written as [18]

$$n_e = \frac{B_\star m_e^3}{2\pi^2} \sum_{\nu=0}^{\nu_{\text{max}}} g_\nu x_e(\nu). \quad (5)$$

where $x_e(\nu) \equiv \sqrt{(\mu_e/m_e)^2 - 1 - 2\nu B_\star}$ and $g_\nu = 1$ for $\nu = 0$ and $g_\nu = 2$ for $\nu \neq 0$.

Regarding the lattice energy $\varepsilon_l(A, Z; P, B)$, it is known to be independent of the magnetic field [12]. Thus, results obtained for $B = 0$ can be safely used here [23]. The most energetically favorable configuration for the outer crust is the crystallization of nuclei into a body-centered cubic lattice [24]. The lattice energy per baryon can be written as

$$\varepsilon_l = -C_l x^2 y^2 p_F, \quad (6)$$

where C_l is a dimensionless constant, $C_l = 3.40665 \times 10^{-3}$ for a body-centered-cubic lattice in our units, $x \equiv A^{1/3}$ is proportional to the size of the nuclei at the vertices of the lattice, $y \equiv Z/A$ is their proton fraction and $p_F \equiv (3\pi^2 n)^{1/3}$ is the average Fermi momentum defined from the average baryon density n .

In our approach, $\varepsilon_n(A, Z)$ do not contribute to the pressure and it is not affected by the magnetic field. This latter statement is certainly valid for magnetic field strengths lower than 10^{17} G [15, 17]. As shown in [16, 17], for some typical nuclei appearing in the outer crust, the presence of $B \approx 10^{17-18}$ G produces a small nuclear extra-binding, favoring the stability of the nuclei present in the lattice. Due to this, the effect of B on the nuclear binding is not expected to impact on our qualitative conclusions concerning the synthesis of SHEs and the underlying mechanism favoring their appearance.

For the sake of completeness, in Appendix A, we give the set of equations needed to obtain the optimal composition of the outer crust briefly explaining the method for the solution. More details can be also found in [16, 18].

In Sec. III, we will adopt two state-of-the-art nuclear models of different type to account for the nuclear energy per baryon (ε_n). In particular, we will consider two Energy Density Functionals (EDFs), one relativistic and one non-relativistic.

II.1. The case of large fields and large densities

In the current section, we will resort to a simplified nuclear mass model in order to shed some light, in a clear and transparent way, on the mechanism triggering the appearance of SHEs. For this illustrative purpose, we have adopted the well-known Liquid Drop Model (LDM), according to which the nuclear energy per baryon can be

written as follows

$$\begin{aligned}\varepsilon_n(x, y) &= m_p y + m_n(1 - y) + \varepsilon_v + \varepsilon_s + \varepsilon_c + \varepsilon_{\text{asym}} \\ &= m_p y + m_n(1 - y) - a_v + \frac{a_s}{x} + a_c x^2 y^2 \\ &\quad + a_a(1 - 2y)^2.\end{aligned}\quad (7)$$

The coefficients $a_v = 15.71511$ MeV, $a_s = 17.53638$ MeV, $a_c = 0.71363$ MeV, $a_a = 23.37837$ MeV are associated to the volume term ε_v , the surface term ε_s , the Coulomb interaction term ε_c and the asymmetry term $\varepsilon_{\text{asym}}$, respectively. The numerical values are those from Ref. [25].

As already mentioned, the presence of SHEs has been associated to extremely large magnetic fields, $B \gtrsim 10^{18}$ G, where $\nu_{\text{max}} = 0$ (strongly quantizing magnetic fields, cf. [18]), and to average baryon densities in the innermost part of the outer crust of the order of 10^{-2} fm $^{-3}$ (cf. Fig. 3 in Ref. [22]). In these conditions, $\mu_e \gg m_e$. Hence, the electron chemical potential can be approximated as

$$\mu_e \approx \frac{2\pi^2 n_e}{m_e^2 B_\star} = \frac{2\pi^2 y n}{m_e^2 B_\star} \equiv \frac{2}{3} y \frac{p_F^3}{m_e^2 B_\star}, \quad (8)$$

where we have checked that, in this range, the latter expression is accurate within a 2% with respect to the exact value.

Recalling that the electron contribution to the Gibbs energy per baryon is equal to $y\mu_e$ and that $P_l/n = \varepsilon_l/3$ [18], one can write the Gibbs energy per baryon as a function of p_F ,

$$\begin{aligned}\mu(x, y; p_F, B_\star) &\approx m_p y + m_n(1 - y) \\ &\quad - a_v + \frac{a_s}{x} + a_c x^2 y^2 + a_a(1 - 2y)^2 \\ &\quad + \frac{2}{3} y^2 \frac{p_F^3}{m_e^2 B_\star} - \frac{4}{3} C_l x^2 y^2 p_F.\end{aligned}\quad (9)$$

The latter expression allows us to easily realize that for a *critic* average Fermi momentum $p_F^c \approx 157$ MeV (i.e., for density $n^c \approx 1.7 \times 10^{-2}$ fm $^{-3}$), the nuclear Coulomb and lattice terms cancel each other ($a_c - \frac{4}{3} C_l p_F^c$) $x^2 y^2 \approx 0$, resulting in a Coulomb *screening* effect. In such a situation,

$$\begin{aligned}\mu(x, y; p_F^c, B_\star) &\approx m_p y + m_n(1 - y) \\ &\quad - a_v + \frac{a_s}{x} + a_a(1 - 2y)^2 \\ &\quad + \frac{2}{3} y^2 \frac{(p_F^c)^3}{m_e^2 B_\star}.\end{aligned}\quad (10)$$

As a matter of fact, we emphasize that the role of the lattice term outside these extreme conditions (i.e. $n^{\text{drip}} \lesssim 10^{-4}$ fm $^{-3}$) has been known to be quite limited $\frac{4C_l p_F^{\text{drip}}}{3a_c} \lesssim 0.2$.

In order to find the optimal composition according to the last equation, one must write $\mu(x, y; p_F^c, B_\star)$ as a function of the pressure. To this aim, we first relate the

pressure with the average Fermi momentum as given in Eq. (29) of Ref. [18],

$$P_c \approx \frac{y^2 (p_F^c)^6}{9\pi^2 m_e^2 B_\star}, \quad (11)$$

which is valid for strongly quantizing magnetic fields, and large densities (or $\mu_e \gg m_e$). Writing Eq. (10) as a function of the pressure, we obtain

$$\begin{aligned}\mu(x, y; P_c, B) &\approx m_p y + m_n(1 - y) \\ &\quad - a_v + \frac{a_s}{x} + a_a(1 - 2y)^2 \\ &\quad + 2\pi \frac{y}{m_e} \left(\frac{P_c}{B_\star} \right)^{1/2}.\end{aligned}\quad (12)$$

From this equation, we first note that the different terms depend only either on the proton fraction $y = Z/A$ or on the mass number $x = A^{1/3}$. This implies that the optimal value of y will be independent of x and vice versa. Specifically, the optimal value of x can be obtained by minimizing $\mu(x, y; P_c, B)$ with respect to x

$$0 = \frac{\partial \mu}{\partial x} = -\frac{a_s}{x^2}, \quad (13)$$

which implies that $x = A^{1/3} \rightarrow \infty$, showing clearly the underlying mechanism triggering the appearance of SHEs. We stress again that this result can be only realized thanks to the presence of the lattice contribution. When considering microscopic calculations for ε_n in Sec. III, this scenario may not be precisely reached, since the Coulomb screening effect may not be perfectly realized.

Regarding the proton fraction y , since the asymmetry term a_a , that favors $y \rightarrow 1/2$, is not opposed by the nuclear Coulomb term, that favors $y \rightarrow 0$, the process of neutron enrichment in this region of the crust is expected to slow down. The limit imposed for the proton fraction in this simple model would be

$$\begin{aligned}0 = \frac{\partial \mu}{\partial y} &= m_p - m_n - 4(1 - 2y)a_a + \frac{2\pi}{m_e} \left(\frac{P_c}{B_\star} \right)^{1/2}, \\ y &\approx \frac{1}{2} - \frac{\pi}{4m_e a_a} \left(\frac{P_c}{B_\star} \right)^{1/2}, \\ y &\approx \frac{1}{2} \frac{1}{1 + \frac{1}{12} \frac{(p_F^c)^3}{m_e^2 a_a B_\star}} \approx 0.33.\end{aligned}\quad (14)$$

Here, the proton-neutron mass difference has been neglected. As we will show in what follows, this simple model leads to reliable qualitative values for x and y , in its regime of applicability.

In Fig. 1 we show the equation of state –the pressure as a function of the number density– predicted by the LDM for $B = 1.0 \times 10^{16}$ G, $B = 1.0 \times 10^{18}$ G, $B = 3.0 \times 10^{18}$ G, $B = 4.4 \times 10^{18}$ G, without making any approximation in the calculation of $\mu(x, y; P, B)$ (solid lines). Results neglecting the Coulomb lattice are also displayed (dashed

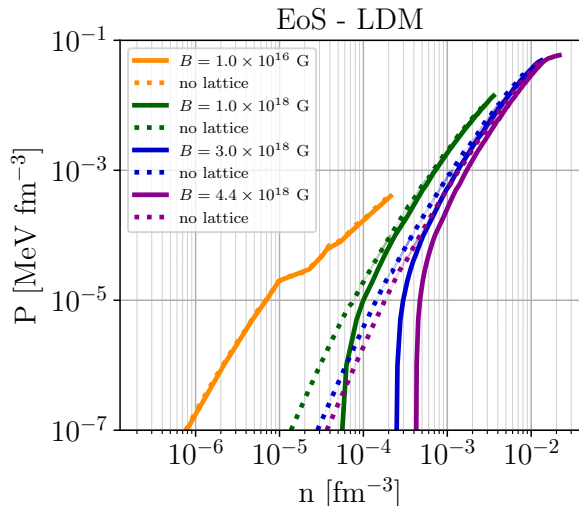


FIG. 1. Equation of state (P versus n) predicted by the LDM, for different external magnetic field values ($B = 1.0 \times 10^{16}$ G, $B = 1.0 \times 10^{18}$ G, $B = 3.0 \times 10^{18}$ G, $B = 4.4 \times 10^{18}$ G), including (solid lines) and neglecting (dashed lines) the contribution of the lattice Gibbs energy. The curves are plotted up to the neutron-drip transition point.

lines). It is evident that $B \gtrsim 10^{18}$ G produces outer crusts with larger densities and pressures before the neutron drip line is reached. In the outermost layer, for the highest magnetic fields where only the $\nu = 0$ electronic level is filled, the density remains almost unchanged for a large range of pressure values, but this does not occur when neglecting the lattice contribution to the pressure. That is, the lattice makes the crust practically incompressible in the outermost layers (cf. Sec. IV.a of Ref. [18]).

For completeness, we show in Fig. 2 our results for the composition of the outer crust, i.e. $Z(n)$ and $N(n)$, either including (upper panels) or neglecting (lower panels) the lattice contribution. The results are for $B = 1.0 \times 10^{16}$ G, $B = 1.0 \times 10^{18}$ G, $B = 3.0 \times 10^{18}$ G, $B = 4.4 \times 10^{18}$ G, from left to right. First, it is important to note that the neutron drip density increases from $\sim 10^{-4}$ fm $^{-3}$ to $\sim 10^{-2}$ fm $^{-3}$ while going from the lowest magnetic field to the most intense one, in agreement with the literature. It is crystal clear, by comparing the upper with the lower panels, that the presence of the lattice contribution is responsible for the strong increase of both Z and A , in of the innermost layers of the outer crust leaving, approximately, the Z/A ratio unchanged (not shown). This is a numerical validation of the analytic model that has been given above.

III. Results

The possible appearance of SHEs was not considered in our previous work [16] due to the limit imposed on

the proton and neutron numbers in the employed mass tables. Moreover, in that work we did not consider magnetic fields whose values extend up to $B \sim 3 - 5 \times 10^{18}$ G.

In this section, we present our results obtained from the numerical minimization of the Gibbs energy per particle, $\mu(A, Z; P, B)$ [cf. Eq. (1)], focusing on the composition based on two state-of-the-art nuclear mass models covering now a larger range of Z values and, consistently, of N values. Specifically, we have employed the relativistic DDPC1 [26] and the non-relativistic UNEDF1 [27] energy density functionals. These mass tables can be found in [28] including the binding energy of nuclei up to $Z \sim 120 - 140$ and covering isotopes from the proton to the neutron drip lines (in the vacuum). In this section, we will pay special attention to the effects produced in the innermost layers of the outer crust, when extremely strong magnetic fields are present. We shall assess how these effects are qualitatively independent of the choice of the model to describe nuclear masses, and consistent with the expectations of the previous subsection.

The nuclear composition of the outer crust, i.e. the functions $Z(n)$ and $N(n)$, are displayed in Figs. 3 and 4 for four different magnetic field values. We show in these figures results corresponding to the UNEDF0 (non-relativistic) and DDPC1 (relativistic) energy density functionals. As previously done in the case of the LDM, we show in the lower panels the results obtained neglecting the lattice contribution. The four selected external magnetic field values are $B = 1.0 \times 10^{16}$ G, $B = 1.0 \times 10^{18}$ G, $B = 3 \times 10^{18}$ G, $B = 5 \times 10^{18}$ G, and they cover the same range studied in Ref. [22].

For the lowest magnetic field, $B \sim 1.0 \times 10^{16}$ G, there are no significant differences with respect to the previous works and to the results obtained by neglecting the lattice contribution. Below $B \approx 10^{18}$ G, we reach maximum values of $Z \approx 60$ and $N \approx 130$, with slight variations according to the chosen nuclear mass model (in agreement with our previous results [16]). The presence of super-heavy and very neutron-rich nuclei emerges from $B \sim 10^{18}$ G and it is evident for the highest analyzed magnetic field $B = 4.4 \times 10^{18}$ G, for densities around $n \sim 10^{-2}$ fm $^{-3}$, as expected from our previous discussion based on the LDM. The aforementioned results are similar for the considered mass models, suggesting that they are robust against the model choice and that the physics mechanism enabling the appearance of SHEs is qualitatively well understood based on the simplified model previously introduced. Indeed, as we have already stressed in the case of the LDM, the calculations neglecting the lattice contribution (lower panels in Figs. 3 and 4), do not predict SHEs to appear in the outer crust.

Another interesting feature of our results is that the predicted SHEs are not particularly unbalanced in the $y = Z/A$ ratio. This constitutes a smoking gun of the slowing down of the electron capture due to the interplay between the Coulomb term that, at the largest densities and magnetic fields, does not oppose to the asymmetry

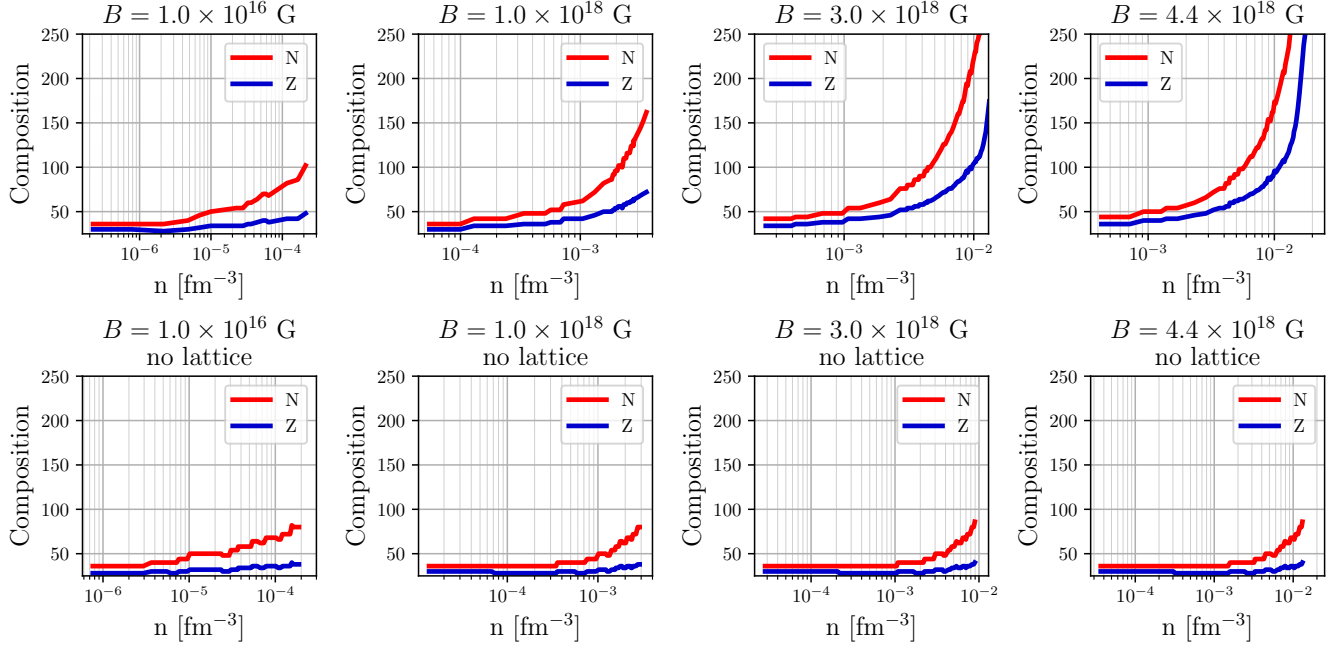


FIG. 2. Composition, i.e. $Z(n)$ and $N(n)$ trends (blue solid line and red solid line respectively), of the outer crust of a magnetar obtained by employing the LDM for the nuclear binding energies, for the following values of magnetic field: $B = 1.0 \times 10^{16}$ G, $B = 1.0 \times 10^{18}$ G, $B = 3.0 \times 10^{18}$ G, $B = 4.4 \times 10^{18}$ G.

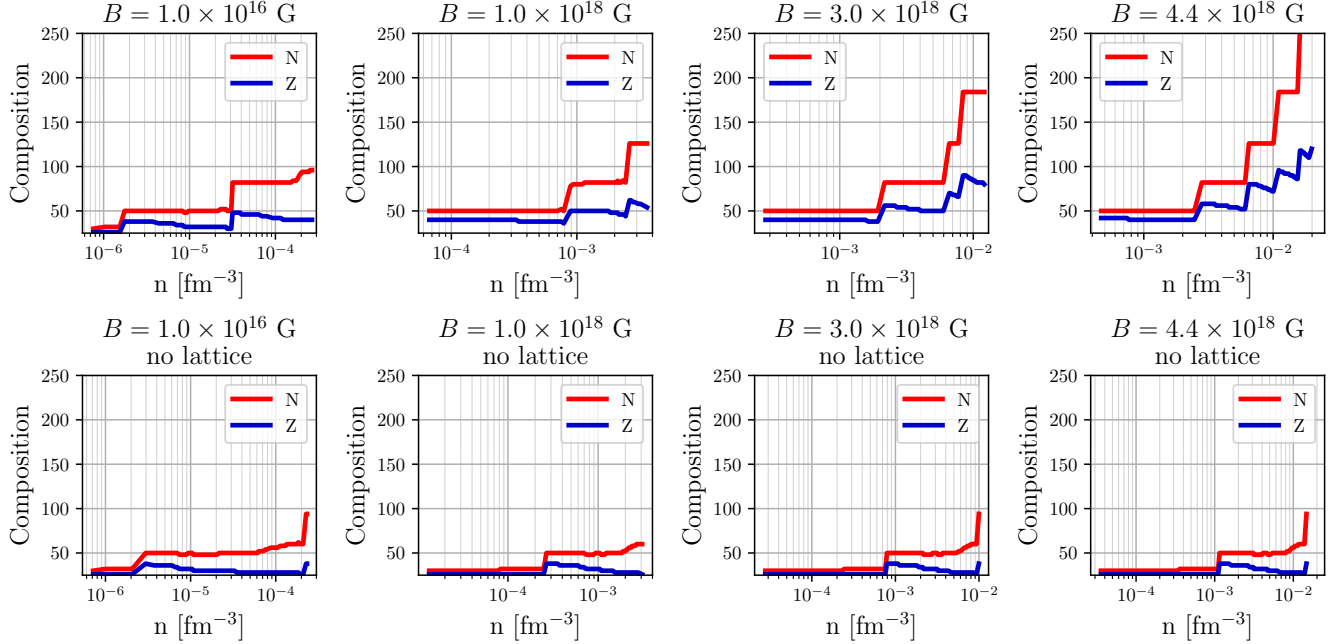


FIG. 3. Compositions, i.e. $Z(n)$ and $N(n)$ trends (blue solid line and red solid line respectively), of the outer crust of a magnetar obtained by employing UNEDF1 model for the nuclei binding energies, for the following values of magnetic field: $B = 1.0 \times 10^{16}$ G, $B = 1.0 \times 10^{18}$ G, $B = 3.0 \times 10^{18}$ G, $B = 5.0 \times 10^{18}$ G.

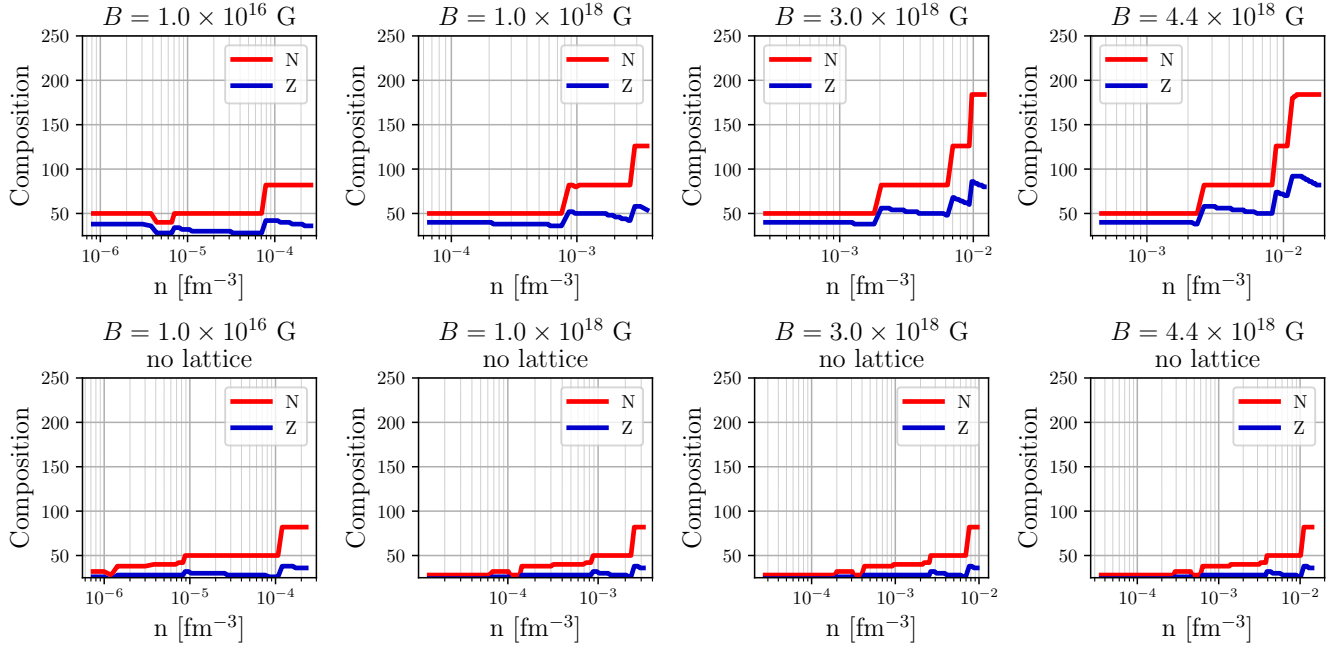


FIG. 4. Compositions, i.e. $Z(n)$ and $N(n)$ trends (blue solid line and red solid line respectively), of the outer crust of a magnetar obtained by employing the DDPC1 model for the nuclei binding energies, for the following values of magnetic field: $B = 1.0 \times 10^{16}$ G, $B = 1.0 \times 10^{18}$ G, $B = 3.0 \times 10^{18}$ G, $B = 5.0 \times 10^{18}$ G.

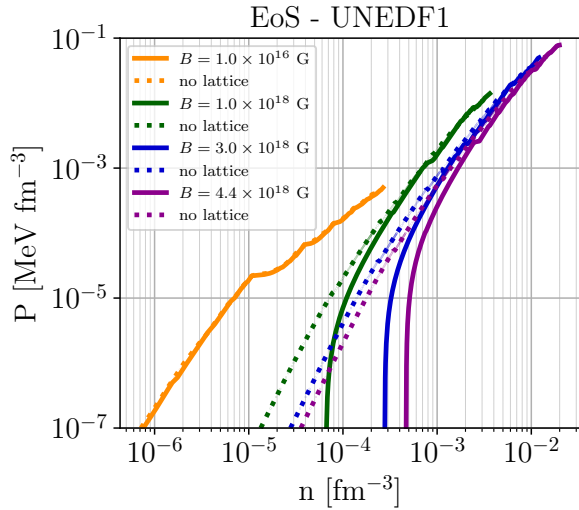


FIG. 5. Equation of state (P versus n) predicted by the UNEDF1 model, for different external magnetic field values ($B = 1.0 \times 10^{16}$ G, $B = 1.0 \times 10^{18}$ G, $B = 3.0 \times 10^{18}$ G, $B = 4.4 \times 10^{18}$ G), including (solid lines) and neglecting the contribution of the lattice Gibbs energy (dashed lines). Curves are plotted up to the neutron-drip transition point.

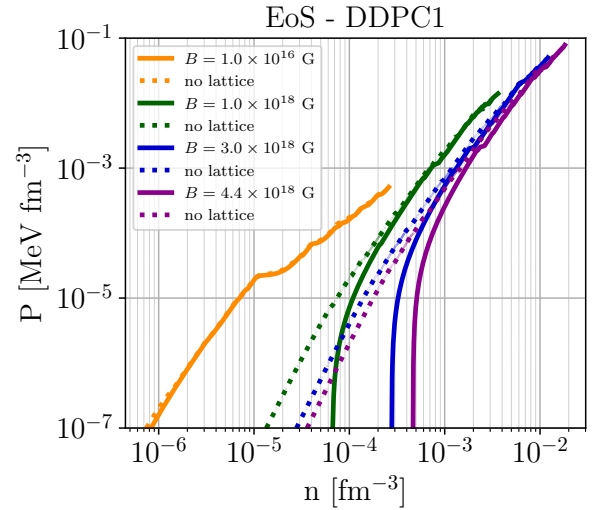


FIG. 6. Equation of state (P versus n) predicted by the DDPC1 model, for different external magnetic field values ($B = 1.0 \times 10^{16}$ G, $B = 1.0 \times 10^{18}$ G, $B = 3.0 \times 10^{18}$ G, $B = 4.4 \times 10^{18}$ G), including (solid lines) and neglecting the contribution of the lattice Gibbs energy (dashed lines). Curves are plotted up to the neutron-drip transition point.

term leading to a tug of war between the electron energy contribution, that would favor $y \rightarrow 0$, and the asymmetry term in the mass models, that would favor $y \rightarrow 1/2$.

For the sake of completeness, we display in Figs. 5

and 6 the equation of state associated with the UNEDF1 and DDPC1 mass models for $B = 1 \times 10^{15}$ G, $B = 1 \times 10^{17}$ G, $B = 1 \times 10^{18}$ G, $B = 3 \times 10^{18}$ G (solid lines). Results neglecting the Coulomb lattice are also displayed

(dashed lines). There are small differences between the results of UNEDF1 and DDPC1, although they cannot be visible on the overall scale. Similar results have been found previously [16–21].

We have checked that at least two more mass models that have been extended up to $Z \sim 120 - 140$ and cover isotopes from the proton to the neutron drip lines (in the vacuum), namely HFB-32 [29] and UNEDF0 [30], provide similar results for the crust compositions.

IV. Conclusion

In the present work, we have analyzed again, and in more detail, the nuclear composition of the outer crust of neutron stars that are characterized by strong magnetic fields (magnetars). This topic has been already the subject of different works and yet, for the first time, the work of Ref. [22] has found, unexpectedly, that when those magnetic fields are larger than $\approx 10^{18}$ G, SHEs can be found in the innermost layers. In our current paper, we have found a clear explanation for this mechanism, and discussed further important aspects.

First, we have confirmed the existence of SHEs by using two state-of-the-art nuclear mass models. A physical interpretation for the synthesis of such elements is given in a transparent way, based on the LDM. Realistic calculations qualitatively follow the trends expected by our simplified analysis using the LDM, and confirm the insight that is gained thanks to this robust, albeit simple, model.

In essence, magnetic fields above 10^{18} G quantize the energies of the ionized electrons, and allow them to reach larger Fermi momenta, with respect to the case of the free electron gas. This enables the presence of densities of around 10^{-2} fm^{-3} within the outer crust. We have clearly shown that this density leads to an unusual situation in which the contribution of the electron lattice to the average chemical potential tends to quench, or even cancels, the effect of the nuclear Coulomb term. This situation gives more freedom to the asymmetry term, that opposes more efficiently the increase with density of the electronic contribution to the average chemical potential, by slowing down the neutron enrichment of the outer crust. The role played by the lattice term to the Gibbs energy per baryon, for the largest densities and magnetic fields analyzed, turns out to be decisive. Eventually, in this situation, the most convenient way of optimizing the chemical potential is by decreasing the nuclear surface

energy by allowing nuclei to be more and more heavy.

Although this mechanism cannot be trivially replicated in terrestrial laboratories, it sheds some interesting light on the physics of SHEs and their synthesis. The very concepts of nuclear stability, drip lines and/or highest possible atomic number, is strongly altered in the medium that may exist in magnetars, provided magnetic fields of the order of $\approx 10^{18}$ G can be reached.

Acknowledgments

We would like to thank Prof. Sekizawa for bringing into our notice the possible appearance of superheavy elements in the outer crust of extremely magnetized neutron stars. XRM acknowledge support by grants PID2020-118758GB-I00 funded by MCIN/AEI/10.13039/501100011033; by the “Unit of Excellence María de Maeztu 2020-2023” award to the Institute of Cosmos Sciences, Grant CEX2019-000918-M funded by MCIN/AEI/10.13039/501100011033; and by the Generalitat de Catalunya, grant 2021SGR01095.

A. Algorithm to find the composition of the crust

In a nutshell, to determine the outer crust composition, that is to seek for the optimal nucleus, we solve consistently the following set of equations, that determine μ_e , ν_{\max} , n_e , $p_e^F(\nu)$ [16]:

$$\begin{cases} \mu_e^2 = m_e^2 (1 + 2\nu_{\max} B_\star), \\ p_e^F(\nu)^2 + m_e^2 (1 + 2\nu B_\star) = \mu_e^2, & 0 \leq \nu \leq \nu_{\max}, \\ n_e = \frac{B_\star m_e^3}{2\pi^2} \sum_{\nu=0}^{\nu_{\max}} g_\nu x_e(\nu), \\ P = P_e + P_l(A, Z). \end{cases} \quad (\text{A1})$$

Since the four coupled equations (A1) cannot be solved analytically, we have adopted a numerical procedure to solve (A1) for a given magnetic field B and for a fixed pressure P , which can be summarized as follows. First of all, we enter a tentative chemical potential μ_e . From this, we extract ν_{\max} , n_e , and the $(\nu + 1)$ values of $p_{\text{Fe}}(\nu)$ from the first three equations. Inserting these quantities and the input values of Z and A , $P_e + P_l$ is determined. The best μ_e value is the one making the right-hand term of the fourth equation equal to the input pressure. As a consequence, the Gibbs energy (Eq. 1) can be calculated. This procedure is repeated for each Z and A values of interest, and the best pair of values Z , A are those which minimize the Gibbs energy (Eq. 1).

[1] P. Haensel, A. Y. Potekhin, and D. G. Yakovlev, *Neutron stars 1: Equation of state and structure*, Vol. 326 (Springer, New York, USA, 2007).

[2] J. H. Seiradakis and R. Wielebinski, *The Astronomy and Astrophysics Review* **12**, 239 (2004).

[3] C. Y. Ng and V. M. Kaspi, *AstroPhysics of Neutron Stars 2010: A Conference in Honor of M. Ali Alpar*, *American*

- Institute of Physics Conference Series, **1379**, 60 (2011), [arXiv:1010.4592 \[astro-ph.HE\]](#).
- [4] S. Mereghetti, *Astron. Astrophys. Rev.* **15**, 225 (2008), [arXiv:0804.0250 \[astro-ph\]](#).
- [5] S. A. Olausen and V. M. Kaspi, *The Astrophysical Journal Supplement Series* **212**, 6 (2014).
- [6] A. Tiengo, P. Esposito, S. Mereghetti, R. Turolla, L. Nobili, F. Gastaldello, D. Götz, G. L. Israel, N. Rea, L. Stella, S. Zane, and G. F. Bignami, *Nature* **500**, 312 (2013).
- [7] L. Stella, S. Dall’Osso, G. Israel, and A. Vecchio, *Astrophys. J. Lett.* **634**, L165 (2005), [arXiv:astro-ph/0511068](#).
- [8] A. Y. Potekhin and D. G. Yakovlev, *Astronomy and Astrophysics* **314**, 341 (1996), [arXiv:astro-ph/9604130 \[astro-ph\]](#).
- [9] A. Y. Potekhin, *Astronomy and Astrophysics* **351**, 787 (1999), [arXiv:astro-ph/9909100 \[astro-ph\]](#).
- [10] V. M. Kaspi and A. Beloborodov, *Ann. Rev. Astron. Astrophys.* **55**, 261 (2017), [arXiv:1703.00068 \[astro-ph.HE\]](#).
- [11] S. L. Shapiro and S. A. Teukolsky, *Black holes, white dwarfs, and neutron stars: The physics of compact objects* (1983).
- [12] J. H. Van Vleck, *The theory of electric and magnetic susceptibilities* (Oxford University Press, London, 1932).
- [13] I. I. Rabi, *Zeitschrift für Physik* **49**, 507 (1928).
- [14] L. Landau, *Zeitschrift für Physik* **64**, 629 (1930).
- [15] D. Peña Arteaga, M. Grasso, E. Khan, and P. Ring, *Phys. Rev. C* **84**, 045806 (2011).
- [16] D. Basilico, D. P. n. Arteaga, X. Roca-Maza, and G. Colò, *Phys. Rev. C* **92**, 035802 (2015), [arXiv:1505.07304 \[nucl-th\]](#).
- [17] J. Wei and C. Yanjun, (2024), [arXiv:2403.10227 \[nucl-th\]](#).
- [18] N. Chamel, R. L. Pavlov, L. M. Mihailov, C. J. Velchev, Z. K. Stoyanov, Y. D. Mutafchieva, M. D. Ivanovich, J. M. Pearson, and S. Goriely, *Phys. Rev. C* **86**, 055804 (2012).
- [19] N. Chamel, Z. K. Stoyanov, L. M. Mihailov, Y. D. Mutafchieva, R. L. Pavlov, and C. J. Velchev, *Phys. Rev. C* **91**, 065801 (2015).
- [20] V. Parmar, H. C. Das, M. K. Sharma, and S. K. Patra, *Phys. Rev. D* **107**, 043022 (2023), [arXiv:2211.07339 \[astro-ph.HE\]](#).
- [21] N. Chamel and Z. K. Stoyanov, *Phys. Rev. C* **101**, 065802 (2020).
- [22] K. Sekizawa and K. Kaba, Possible existence of extremely neutron-rich superheavy nuclei in neutron star crusts under a superstrong magnetic field (2023), [arXiv:2302.07923 \[nucl-th\]](#).
- [23] G. Baym, C. Pethick, and P. Sutherland, *Astrophysical Journal* **170**, 299 (1971).
- [24] A. Fetter and J. Walecka, *Quantum Theory of Many-particle Systems*, Dover Books on Physics (Dover Publications, 2003).
- [25] X. Roca-Maza and J. Piekarewicz, *Phys. Rev. C* **78**, 025807 (2008).
- [26] T. Nikšić, D. Vretenar, and P. Ring, *Phys. Rev. C* **78**, 034318 (2008).
- [27] M. Kortelainen, J. McDonnell, W. Nazarewicz, P.-G. Reinhard, J. Sarich, N. Schunck, M. V. Stoitsov, and S. M. Wild, *Phys. Rev. C* **85**, 024304 (2012).
- [28] <https://massexplorer.frib.msu.edu>.
- [29] S. Goriely, N. Chamel, and J. M. Pearson, *Phys. Rev. C* **93**, 034337 (2016).
- [30] M. Kortelainen, T. Lesinski, J. Moré, W. Nazarewicz, J. Sarich, N. Schunck, M. V. Stoitsov, and S. Wild, *Phys. Rev. C* **82**, 024313 (2010).